



Numerical Investigation on Aerodynamic Performance and Interaction of a Lift-Offset Coaxial Rotor in Forward Flight

Haotian Qi^{1,2} · Ping Wang¹ · Linsong Jiang¹

Received: 1 September 2021 / Revised: 27 October 2021 / Accepted: 5 January 2022 / Published online: 1 March 2022
© The Author(s), under exclusive licence to The Korean Society for Aeronautical & Space Sciences 2022

Abstract

A numerical method based on Reynolds Averaged Navier–Stokes (RANS) equations and moving overset mesh technique is developed to simulate the unsteady flow field of a rigid coaxial rotor. A high-efficient hybrid trim model is adopted to ensure the simulation accuracy of lift-offset (LOS). Cases in different advance ratios are trimmed for constant thrust coefficient and torque-balance. The effects of LOS, rotor spacing and RPM on the aerodynamic performance and interaction are analyzed. Results show that, in forward flight the lift–drag ratio can be improved by appropriate LOS. The rotor drag increases with LOS, as there is also a corresponding offset of drag. The optimum LOS varies with flight speed. At large advance ratio the interactions of the coaxial rotor are much weak, except the blade–meeting interaction. The interaction is typically illustrated by the impulsive loads of the upper blade at retreating side (270°), as the flow field is dominated by the advancing blade (90°) of the lower rotor. The interaction intensity is sensitive to LOS, rotor spacing and RPM, as it depends on the flow field gradient induced by the lower blade acting on the upper blade.

Keywords Helicopter · Coaxial rotor · Lift-offset · CFD · Forward flight

List of symbols

c	Blade chord
C_T, C_Q	Rotor thrust and torque coefficient
C_L, C_D	Rotor lift and drag coefficient
Cl	Blade sectional lift coefficient
C_p	Pressure coefficient
μ	Rotor advance ratio
Ma_{tip}	Rotor tip Mach number in hover
R	Rotor radius
$\theta_0, \theta_{1s}, \theta_{1c}$	Collective, lateral cyclic, and longitudinal cyclic pitch angles
$S1, U1, L1$	One blade of the single, upper and lower rotors

Subscripts

L	Lower rotor
U	Upper rotor

1 Introduction

Rigid coaxial rotor compound helicopter has been a potential configuration for the next generation of vertical flight aircraft [1], with the increasing requirement of high-speed flight. Sikorsky Aircraft developed the X2 Technology Demonstrator (X2TD) aircraft [2], adopting the advancing blade concept (ABC) [3]. X2TD has shown good capability to achieve higher flight speed while still maintaining hover and low-speed efficiencies. Its coaxial rotor system consists of two contra-rotating rigid rotors. Lateral lift-offset (LOS) is utilized to fully take advantage of the lift potential at the advancing side. At high speed, the rotor thrust is mainly provided by the advancing side, while the retreating side is offloaded. Both the aerodynamic performance, and the interaction feature of rigid coaxial rotor would be affected by LOS.

✉ Haotian Qi
qhtwld@163.com

✉ Ping Wang
pingwang@ujs.edu.cn

¹ Institute for Energy Research, Jiangsu University, Zhenjiang 212013, China

² Key Laboratory of Aerodynamic Noise Control, China Aerodynamics Research and Development Center, Mianyang 621000, China

Some comprehensive analysis softwares based on vortex method, such as RCAS [1, 4], UMARC [5, 6] and CAMRAD II [7–9], have been applied to investigate the effect of LOS on coaxial rotor aerodynamic performance. Those researches can provide valuable aerodynamic data for rigid coaxial rotor helicopter. And the potential of LOS to improve the rotor performance has been verified. However, vortex method is usually built partly based on empirical formulas, which limits its accuracy. At the same time, the detailed interaction flow field cannot be achieved, especially when the upper and lower rotors meet with each other [10]. By comparison, computational fluid dynamics (CFD) method has obvious advantages for the aerodynamic analysis of coaxial rotor.

Lakshminarayan et al. [11] investigated the interaction of a coaxial rotor in hover, using a Reynolds Averaged Navier–Stokes (RANS) solver, OVERTURNS and sliding meshes. The unsteady rotor loads of different rotor spacing was studied. Based on an unsteady RANS solver and moving overset mesh technique, Qi et al. [12, 13] carried out a series of studies on the aerodynamic interaction of coaxial rotor in hover and forward flight. The impulsive fluctuations were explained to be caused by the severe near-field interaction when the upper and lower blades meet with each other [12], which can also be called as blade–meeting interaction. Wang et al. [14] preliminarily studied the aeroacoustic characteristics of a model coaxial rotor. Park et al. [15] investigated the effect of coaxial rotor spacing on interaction in hover and forward flight, based on a RANS solver. However, the rotor pitches were trimmed by CAMRAD II, which was not coupled with the CFD solver. Hayami et al. studied [10] the effect of lift-offset on rotor vibration loads, through a rotorcraft CFD solver rFlow3D. The comprehensive CFD/CSD (computational structural dynamics) loose coupling solver Helios have been applied to coaxial rotor by some researches [16–19]. Among them, Klimchenko et al. [17] conducted some aerodynamic analysis of X2TD in forward flight using CFD and free wake coupled with CSD. The free wake model presented less accurate on the prediction of unsteady rotor loads than the CFD solution. Researches of Jia et al. [18, 19] were focused on the complex types of aerodynamic interaction in forward flight. The impulsive loading-noise of a lift-offset coaxial rotor was interpreted as caused by the blade–crossover interaction.

Present studies are still limited about the influence mechanism of LOS on its aerodynamic performance and unsteady interactions. Especially for the blade–meeting interaction in high-speed forward flight. This paper is a further step of the previous researches [12, 13], which aims to advancing the understanding of rigid coaxial rotor aerodynamics. Current research is focused on the influences of parameter on the aerodynamic performance and unsteady loads of a rigid coaxial rotor. Three parameters are involved, including LOS, rotor spacing and RPM. Here, rotor spacing is pay special interest

as it is a unique design parameter of the coaxial rotorcraft which affects the aerodynamic performance [15, 20]. The work of this paper mainly involves two aspects. One is to figure out the effect mechanism of LOS on rotor performance. The other is to illustrate the interaction characteristics of rigid coaxial rotor in forward flight through the parametric analysis, especially the blade–meeting interaction. The CFD solver used in this paper is developed based on RANS equations. Moving overset mesh is adopted to simulate the rotating and pitching of rotor blades. Cases at different advance ratios are trimmed for certain thrust coefficient, torque-balance and different LOS levels. Trimming is conducted by an efficient CFD/BET (blade element theory) hybrid trim model [13], which is responsible for the CFD solver.

2 Methodology

2.1 CFD Method

The baseline of the CFD solver were developed by the researches [12–14, 21, 22] at Nanjing University of Aeronautics & Astronautics. Navier–Stokes equations [23] are adopted to simulate the rotor flow field, which can be written as

$$\frac{\partial}{\partial t} \iiint_{\partial V} \mathbf{W} dV + \iint_{\partial S} (\mathbf{F}_c - \mathbf{F}_v) \cdot \mathbf{n} dS = 0. \quad (1)$$

Here, the equation is written in finite-volume form, and S and V represent the surface area and volume of a control volume. \mathbf{W} is the vector of conserved variables. \mathbf{F}_c and \mathbf{F}_v are the convective transport quantities and viscous fluxes. Three-order Roe-MUSCL scheme [24, 25] is employed to calculate the inviscid flux terms. The viscous flux terms are evaluated by second-order central difference scheme. The turbulent viscosity is calculated by Spalart–Allmaras turbulence model [26], which is widely used for aircraft rotor and propeller. Dual-time stepping approach is employed for temporal discretization. Implicit LUSGS [27] scheme is used for the calculation of pseudo time step to improve the efficiency.

A moving overset mesh system consists of cartesian background mesh and body-fitted blade mesh. Meshes used in this paper is shown in Fig. 1. The flow field information of the blade and background meshes is exchanged by searching corresponding hole cells and donor elements [22]. Current researches are conducted with a two-bladed model rotor [13]. The parameters of the model rotor are given in Table 1. The blade is formed with constant chord and single airfoil. The rotor tip Mach number (Ma_{tip}) is set as 0.587 for $\mu < 0.4$. The Ma_{tip} is reduced to 0.47 at large advance ratios ($\mu \geq 0.4$) according to the design principle of a rigid coaxial rotor [28]. Meshes are generated to meet the requirement that the

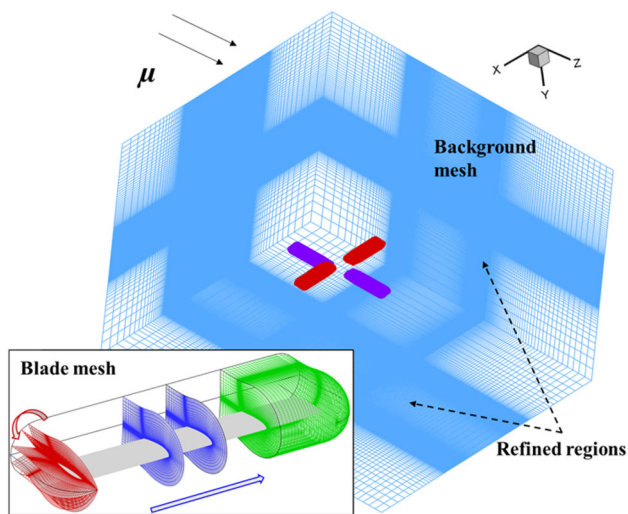


Fig. 1 Sketch map of moving overset mesh for coaxial rotor

Table 1 Parameters of the coaxial rotor model in this paper

Parameter	Values
Rotor radius	2.0 m
Blade cutout	0.212R
Chord	0.22 m
Airfoil	NACA0012
Number of blades	2 + 2
Twist	None
Rotor spacing	0.15R
Rotor shaft tilt angle	0°

mesh size near the blade tip path is refined to about 0.05c, to capture the details of rotor wake. In this paper, the blade mesh has 223 × 89 × 102 points in the streamwise, normal and spanwise directions, respectively. The background mesh has 218 × 196 × 245 points in the directions of x, y and z. The total mesh number is about 14.5 million. The physical time step for one resolution is set as 720, corresponding to a step interval of 0.5° azimuth. And the pseudo time step is set as 15 to ensure the simulation is fully converged, according to the previous calculation experience.

2.2 Trim Model

Pitches of the rigid coaxial rotor are trimmed using a hybrid trim model, which has been built in the previous research. The control settings (x) and target variables (y) are shown below:

$$\begin{aligned}
 \mathbf{x} &= \{\theta_{0U}, \theta_{1sU}, \theta_{1cU}, \theta_{0L}, \theta_{1sL}, \theta_{1cL}\}, \\
 \mathbf{y} &= \{C_T, C_Q, LOS, C_{MU}, C_L, C_{ML}\},
 \end{aligned}
 \tag{2}$$

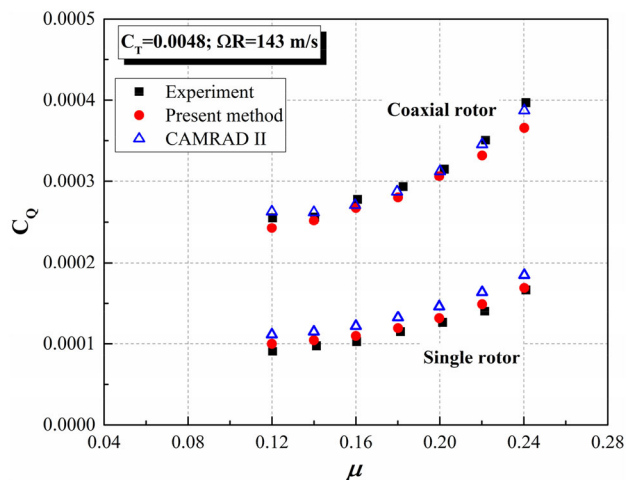


Fig. 2 Comparison of forward flight performances of Harrington rotor-1 [13]

where

$$LOS = |C_{LU} - C_{LL}| / C_T, C_L = C_{LU} + C_{LL}. \tag{3}$$

The detailed description of the trim model can be found in [13, 29]. In trimming, a high-efficiency aerodynamic model based on blade element theory (BET) is coupled with the CFD solver. Trimming process is carried out by the high-efficiency model, which can avoid solving Jacobian matrix through CFD solver. The rotor performance for each trimming iteration step calculated by the BET is modified by the CFD solver. Thus, the efficiency can be significantly improved and the accuracy is guaranteed by the CFD solution.

The hybrid CFD/BET trim model has been validated with various experimental cases in hover and forward flight [12, 13]. The comparison of forward flight performances of Harrington rotor-1 [30] is given in Fig. 2. The performances are calculated with the pitches trimmed for a constant C_T (0.0048). As seen in the figure, the calculation results show good agreements with the results of experiment [30] and CAMRADII [31].

3 Results and Discussion

3.1 Effects of Lift-Offset

To provide accurate control settings for aerodynamic analysis, cases at different flight states are trimmed for C_T = 0.001. The other target values are all zero, except that LOS is set according to demand. Figure 3 shows the trimmed pitch angles for various advance ratios, from 0.1 to 0.5. For mu = 0.1, there are some differences between the pitches of the twin rotors. The difference of longitudinal cyclic pitch (theta_1c) is greater than the collective pitch (theta_0). This is mainly due

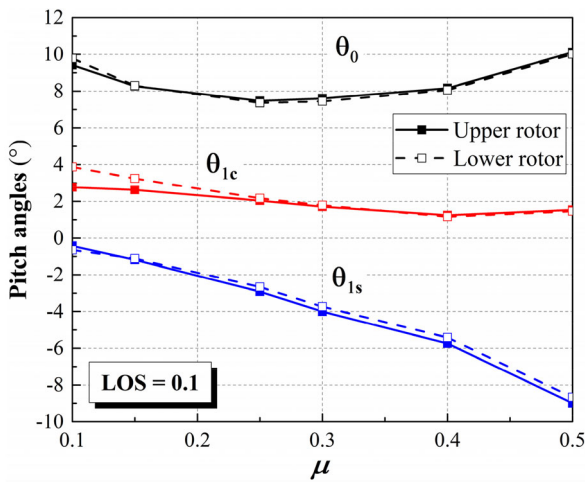


Fig. 3 Trimmed pitches for the rigid coaxial rotor at different advance ratios (LOS = 0.1)

to the strong interaction of the twin rotors at low advance ratio, which enhances the longitudinal asymmetry of the flow field in the rotor disks. To maintain the balance of pitching moment, the difference of θ_{1c} between the twin rotors increases. With the increase of advance ratio, the interaction intensity turns weak, and the collective pitches decrease first and then increase. θ_{1c} decreases in a small amplitude, while θ_{1s} rapidly drops to larger negative values. At high advance ratio, the pitches of the upper and lower rotors tend to be consistent. For $\mu = 0.5$, pitches of the twin rotors are essentially same.

The concept of LOS is proposed to improve the aerodynamic performance of rigid coaxial rotor in high-speed flight. In forward flight the main concerning performance parameter is effective lift–drag ratio (L/De) of rotor [2]. For a single rotor it can be written as

$$L/De = \frac{C_L}{C_D + C_Q/\mu}, \tag{4}$$

where C_L and C_D separately indicate the rotor lift and drag coefficients in the wind axis system. C_Q is the rotor torque coefficient. The denominator term (equivalent drag) consists of drag (C_D) and power equivalent drag (C_Q/μ). The definition of lift–drag ratio for rigid coaxial rotor is similar to the single rotor, where C_L and C_D are the resultant force of the twin rotors and C_Q is the sum of absolute values of rotor torques.

The effect of LOS on performances of the rigid coaxial rotor is shown in Fig. 4. With the increase of LOS, the rotor lift–drag ratio first increases and then decreases. The LOS corresponding to maximum lift–drag ratio varies at different advance ratio states. For $\mu = 0.25$, the optimum LOS is about 0.1, while for $\mu = 0.4$ or 0.5, it is about 0.2. The variation

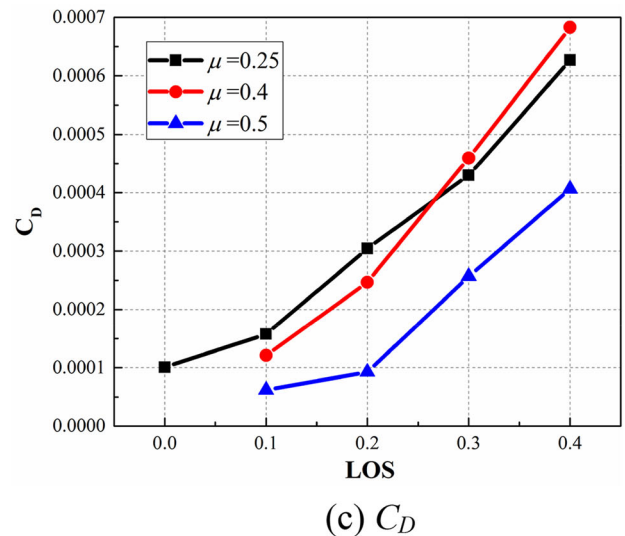
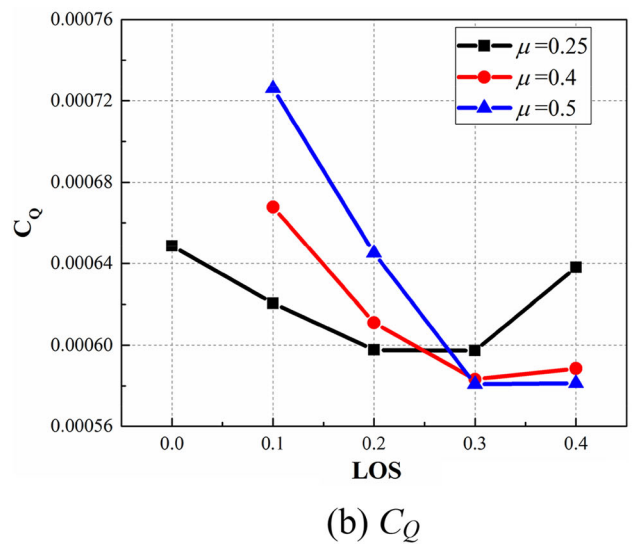
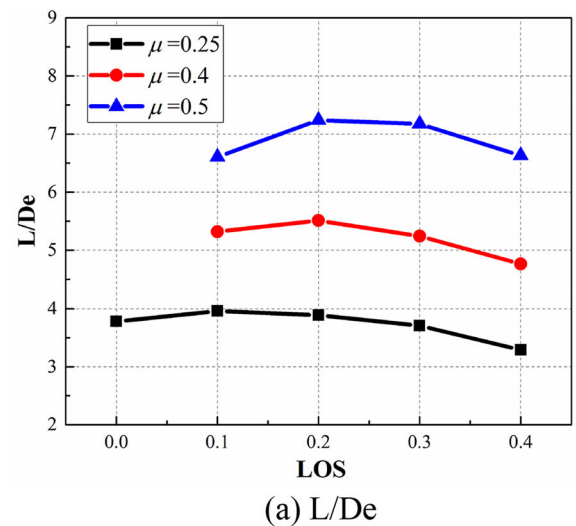


Fig. 4 Performance comparison of rigid coaxial rotor with different LOS

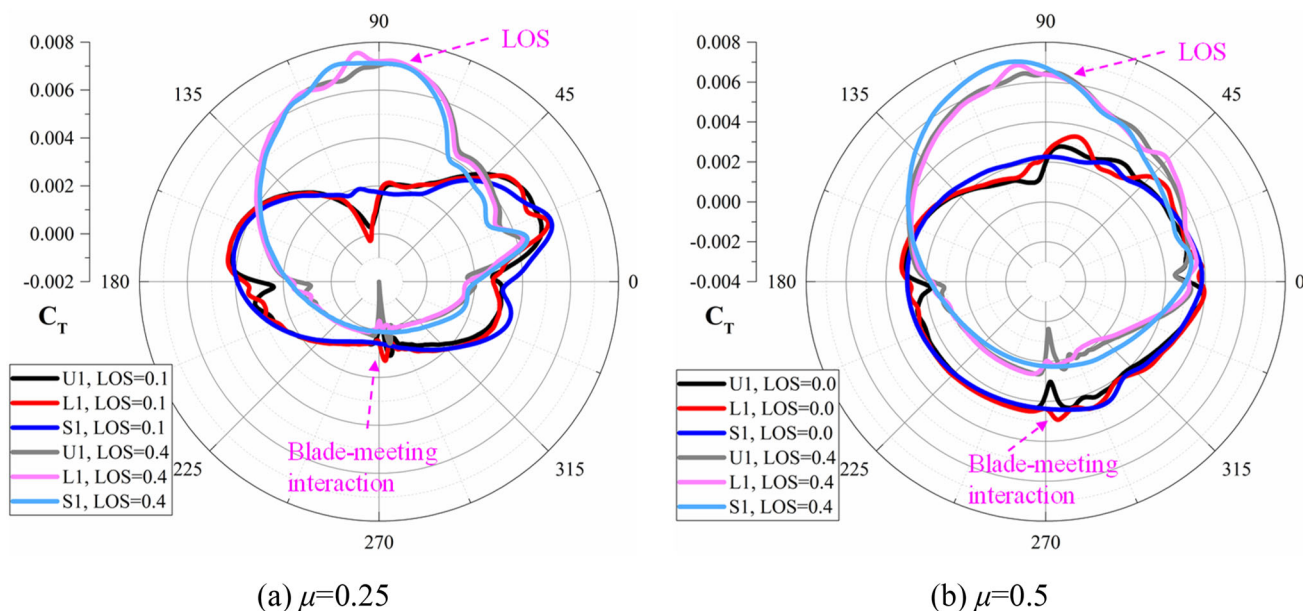


Fig. 5 Temporal blade C_T with different LOS

tendency of lift–drag ratio with LOS parallels the performance test of a rigid coaxial rotor conducted by Deng [15]. As shown in Fig. 4b, for $\mu = 0.25$ the rotor torque reaches the minimum value when $LOS = 0.2$. For $\mu = 0.4$ or 0.5 , the lowest point locates at about $LOS = 0.3$. In summary, a proper LOS can reduce the torque and lift–drag ratio of the rigid coaxial rotor. And higher advance ratio corresponds to larger proper LOS within limits. However, the rotor drag increases with LOS, see Fig. 4c. The reason will be analyzed in detail referring to Fig. 8.

Considering the longitudinal asymmetry of flow field in forward flight, loads of the blade, rather than the rotor are more meaningful for the analysis of unsteady interactions. The temporal blade C_T with different LOS for $\mu = 0.25$ and 0.5 are shown in Fig. 5. Here the results of single rotor configuration are also carried out for comparison. S1, U1, L1, indicate the first blade of the single, upper and lower rotors, separately. And the blade azimuth is shown in polar coordinate for a more intuitive display of LOS. First, compared with hover state, the aerodynamic interaction of rigid coaxial rotor in forward flight is much weaker. With the increase of LOS and advance ratio, the blade thrusts of the coaxial and single rotors tend to be consistent. However, the interaction caused by the blade–meeting event turns more severe. And this is obviously indicated on the C_T of U1 blade at about 270° .

More importantly, the influence of LOS on the rotor load distribution has been illustrated in Fig. 5. For $\mu = 0.25$, $LOS = 0$, the distribution of blade C_T is elliptical. The thrust is large at the longitudinal azimuths (near 0° and 180°), and relatively small at the lateral azimuths (near 90° and 270°).

That is because the dynamic pressure of blade at the retreating side (270°) is much small. Considering the limitation of blade stall, the retreating blade can provide less thrust than the blade at 0° or 180° azimuths. To guarantee the balance of rolling moment, the thrust potential of the advancing blade is suppressed. This is more obvious when $\mu = 0.5$, as higher flight speed will cause larger reverse-flow zone and poorer aerodynamic efficiency at the retreating side. The LOS of a coaxial rigid rotor refers to the offset of the lateral lift. With a larger LOS, the thrust at the advancing side is obviously larger, while at the retreating side, it is rather smaller. Meanwhile, the thrusts at the longitudinal azimuths turns smaller too. In general, the large thrust range is concentrated near the 90° azimuth, which can take full advantage of the large dynamic pressure at the advancing side. In this way, the rotor aerodynamic efficiency in high-speed flight can be improved.

Figure 6 shows the sectional lift distributions ($c_l m a^2$) in the rotor disk for the coaxial and single rotors. The blade–vortex interaction (BVI) events can be found in the advancing side on each rotor disk for the upper and lower rotors, which is consistent with the single rotor. The q-criterion iso-surface of the coaxial rotor at 60° azimuth is shown in Fig. 7. As shown, the vortex shedding from the retreating side blade tip acts on the advancing side blade. For $LOS = 0.4$, the high-lift region mainly lies on the advancing side, while on the retreating side the lift is rather low. And the BVI is significantly enhanced by larger LOS. The lift distributions of the twin rotors are generally similar with the single rotor, except the low-lift regions near blade–meeting azimuths. This is coincident with the analysis referring to Fig. 5.

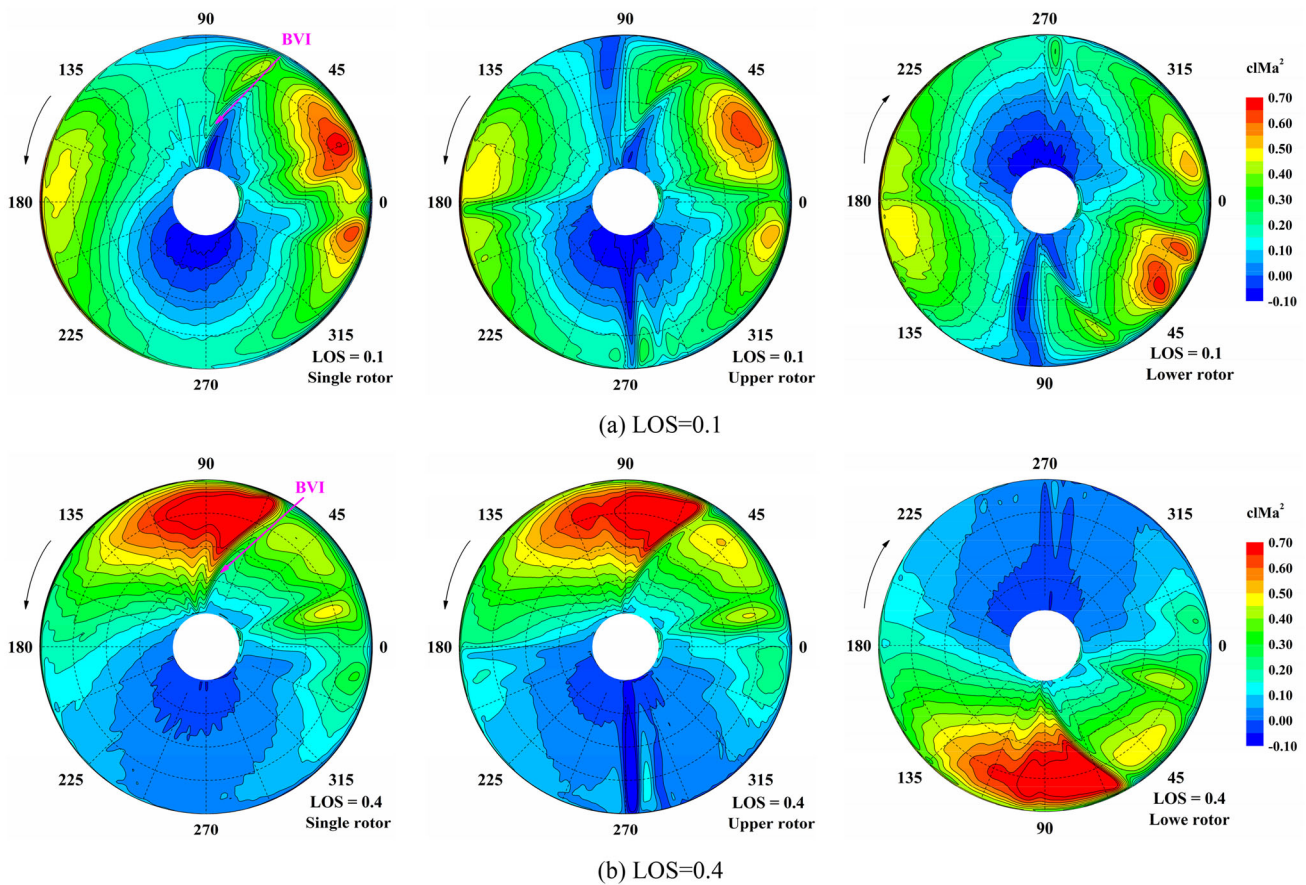


Fig. 6 Sectional lift distributions ($cIMa^2$) in the rotor disk with different LOS ($\mu=0.5$)

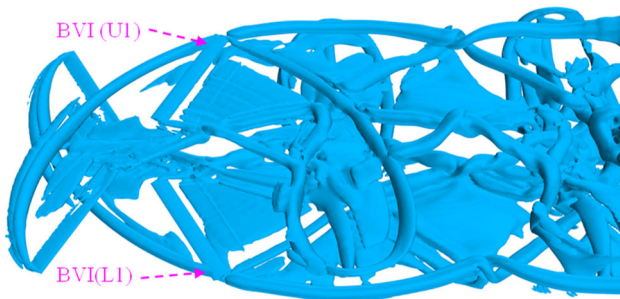


Fig. 7 Q-criterion iso-surface of the coaxial rotor ($\mu=0.5$, $LOS = 0.4$, $q = 0.01$)

The temporal blade drag coefficients with different LOS are given in Fig. 8, to investigate the influence mechanism of LOS on the total rotor drag. The blade C_D stands for the temporal resultant force in the vertical direction of local blade spanwise in the rotor disk plane. For the convenience of comparison, the blade azimuths in this figure are uniformly given in counterclockwise, although the upper and lower rotors rotate in opposite directions. There is obvious impulsive fluctuation near the 270° azimuth, which is still caused by the blade-meeting interaction. The blade drags of

the single and coaxial rotors all gradually deviates toward the advancing side with the increase of LOS, which means that the drag offset appears with the lift-offset. The offset of temporal blade drag distribution will increase the total time-averaged rotor drag. This provides a good explanation for the phenomenon as mentioned in Fig. 4c.

The sectional C_p contours at different azimuths for $\mu=0.5$ are given in Fig. 9, to make a view of the blade-meeting interaction. When the rotors meet at longitudinal azimuths (0° and 180°), the loads of the upper and lower rotors are relatively close. And the flow field is not dominated by either side. When the upper blade (U2) locating at 270° meets the lower blade (L1) at 90° , the flow field is obviously dominated by L1, as it owns much larger dynamic pressure and stronger load than U2. Similarly, the flow field is dominated by U1 90° at rather than L2 at 270° . However, the flow field gradient above the blade is stronger than the below, so the load fluctuations caused by the blade-meeting interaction are more obviously shown by the loads of the upper blade at 270° azimuth.

With the increase of LOS, the attack angle and loads of L1 turn larger. The negative-pressure region above the blade is further enhanced. The enhancement of the negative-pressure

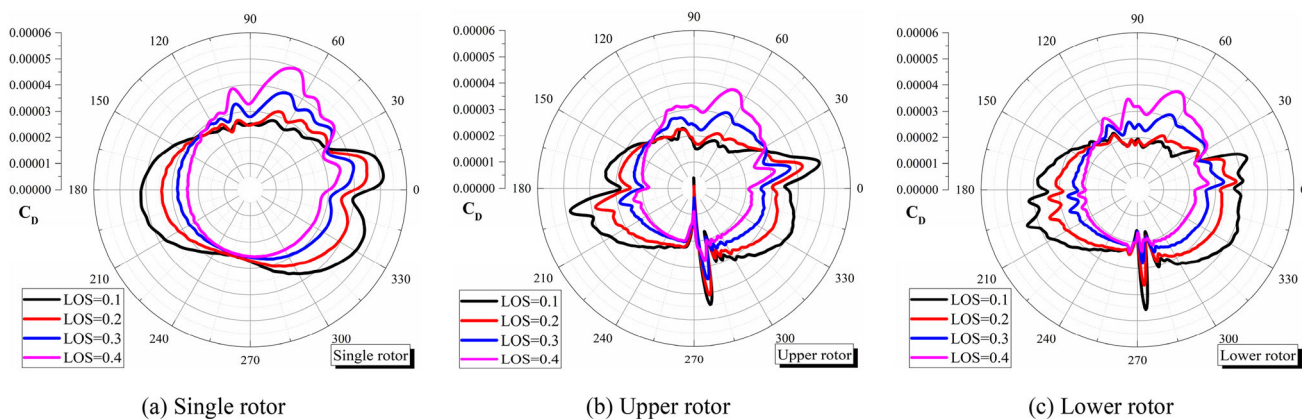


Fig. 8 Temporal blade C_D for different LOS ($\mu = 0.5$)

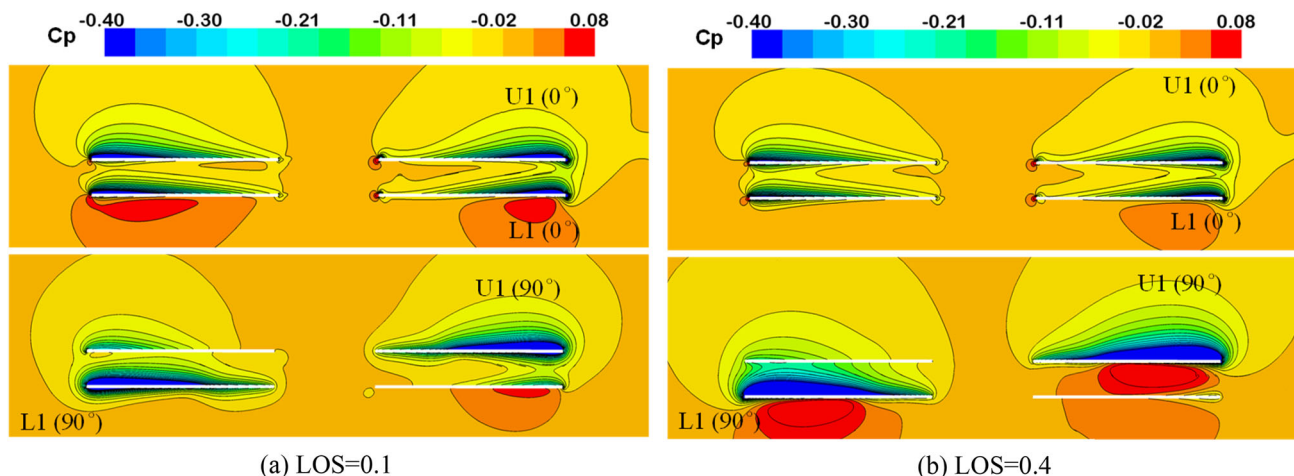


Fig. 9 Sectional C_p contours at 0° and 90° azimuths for different LOS ($\mu = 0.5$)

region below is relatively insignificant. Therefore, the interaction from L1 to U2 turns stronger, while the interaction from U1 to L2 turns weaker. And this is corresponding to the amplitudes of the upper and lower blades as shown in Fig. 5.

3.2 Effects of Rotor Spacing and RPM

As mentioned above, at high-speed flight, the most obvious interaction between the upper and lower rotors is the blade-meeting interaction. In this section, the effects of rotor vertical spacing and RPM are investigated for $\mu = 0.5$. Figure 10 shows the comparison of temporal blade C_T for the coaxial rotor blades with different rotor spacing. Here, the original spacing of the coaxial rotor is marked as H. For LOS = 0.1, the differential C_T fluctuations with the single rotor mainly lie in two ranges, one is at about $90^\circ \sim 95^\circ$ marked as #1. Another is near the blade-meeting azimuths, which is much obvious for the upper rotor at 180° and 270° marked as #2. The amplitude of #1 and #2 fluctuations both turn weak. #2 fluctuation is recognized as the blade-meeting interaction, and gradually disappears with the increase of

rotor spacing. However, for the #1 fluctuation, there is still some difference with the single rotor when the rotor spacing is $2.0H$. This indicates that it is caused by other kind of interaction which is not insensitive to the rotor spacing. For LOS = 0.4, and the thrusts of the coaxial and single rotors are generally consistent, except for the blade-meeting azimuths. The effect of rotor spacing mainly locates near 270° azimuth, where the impulsive amplitude of C_T gradually turns small. And the effect is more obvious shown on the upper rotor than the lower rotor.

Figure 11 shows the temporal blade C_T of different LOS at a higher RPM, $Ma_{tip} = 0.588$. The general fluctuation characteristics are similar with the low RPM case. The main difference locates near 270° azimuth. First, the fluctuation amplitudes of the upper and lower blades are larger. Second, the waveform is different. There is an obvious secondary fluctuation (#2) after the main fluctuation (#1). Blade section lifts at three spanwise locations with different RPM are given in Fig. 12. As the section moves from inboard to outboard, the linear velocity increases and the effect of RPM turns greater. Compared with the 0.4R section, the lift fluctuation

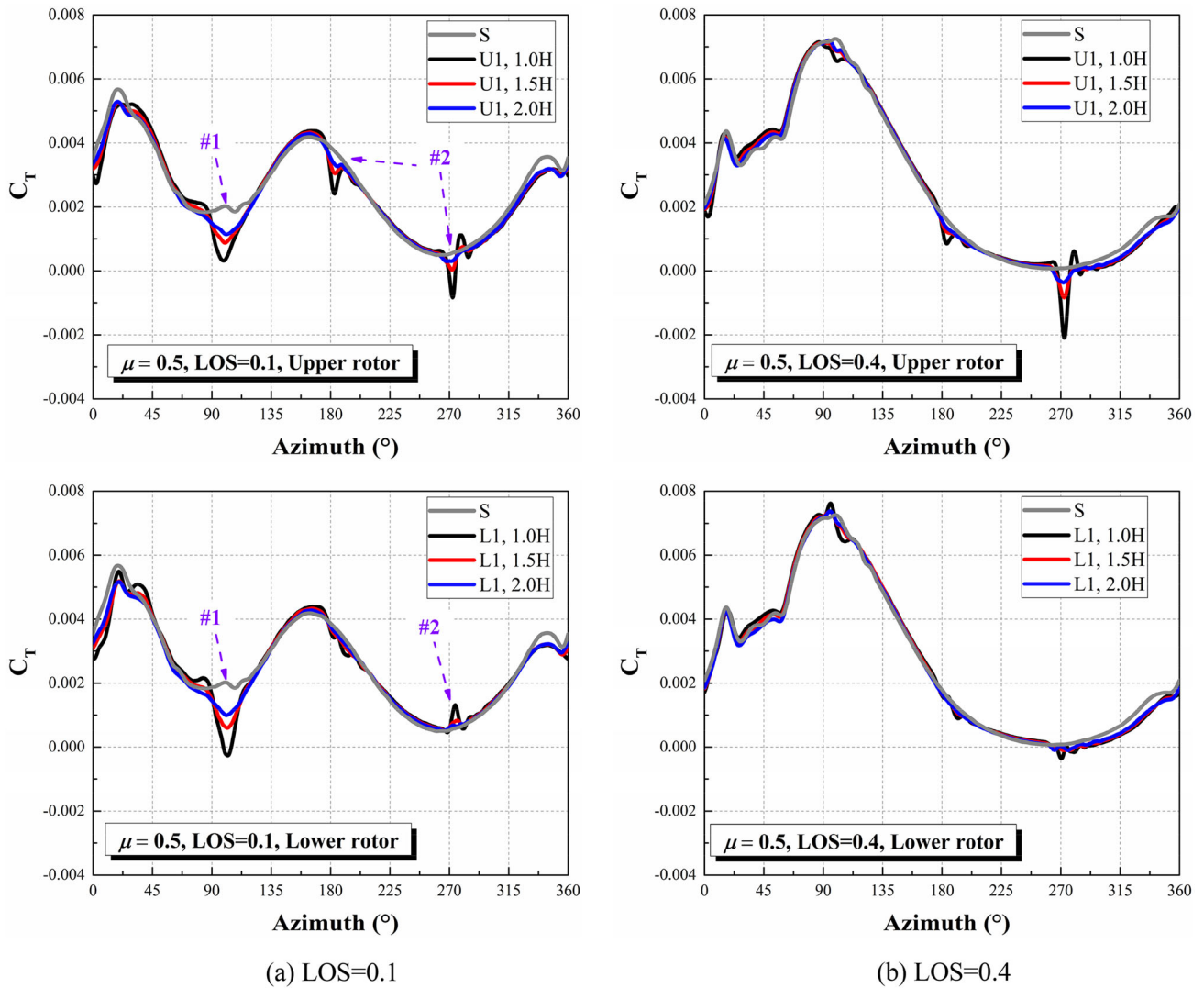


Fig. 10 Temporal blade C_T of different rotor spacing ($\mu = 0.5$)

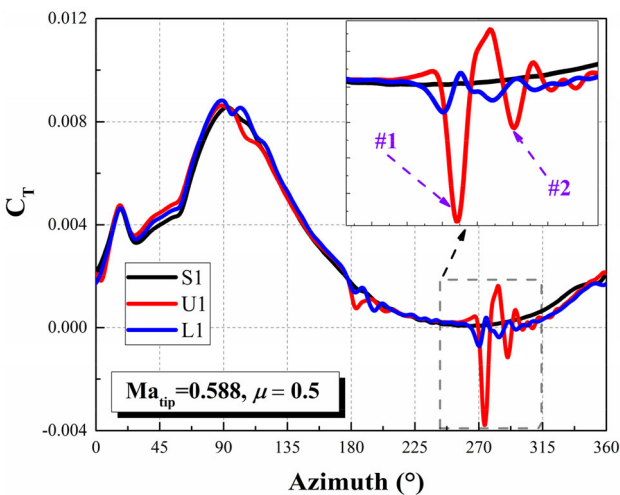


Fig. 11 Temporal blade C_T at a high RPM ($Ma_{tip} = 0.588$, $\mu = 0.5$, $LOS = 0.4$)

of 0.9R is magnified severely near 270°, which dominates the fluctuation of the blade thrust. The BVI at the advancing side is also shown by the section lifts from 45° to 90°. And it is also enhanced with higher RPM, especially at 0.9R. When $Ma_{tip} = 0.588$, the local Mach number of the advancing blade tip is close to 0.882, and weak shock waves are generated in the flow field, as shown in Fig. 13. Thus, the gradient of the flow field above the blade turns greater and shows some different distribution characteristics, compared with the case at low RPM.

4 Conclusions

The aerodynamic performance and unsteady loads of a coaxial rotor model at different advance ratios are investigated, using an unsteady RANS solver based on moving overset

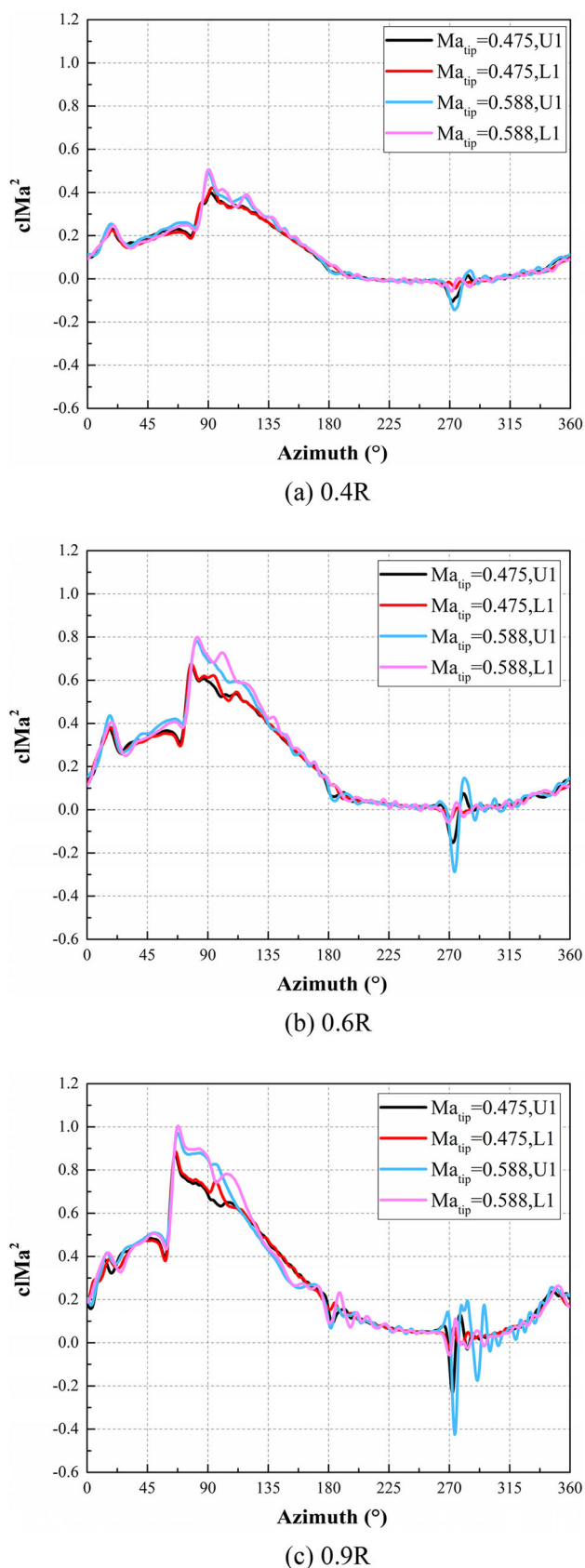


Fig. 12 Temporal blade section lifts at different RPM ($\mu = 0.5$, LOS = 0.4)

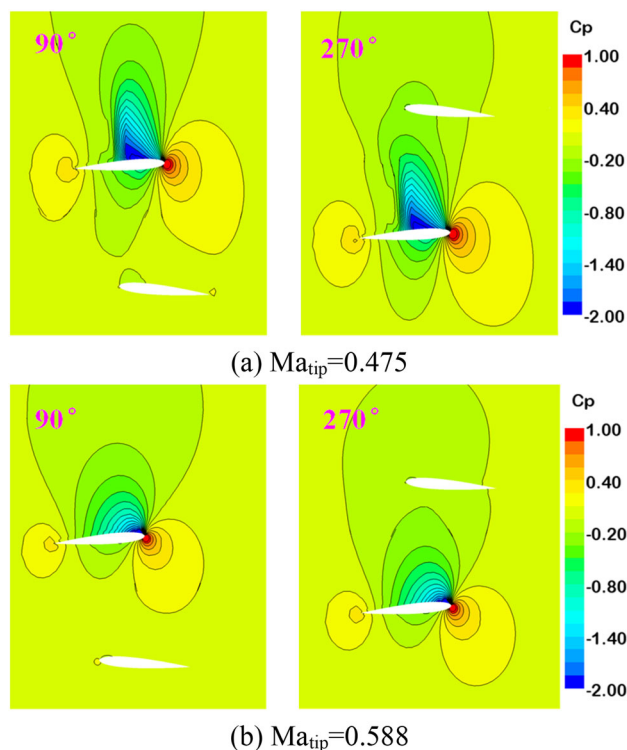


Fig. 13 Sectional C_p contours of 0.9R at different RPM ($\mu = 0.5$, LOS = 0.4)

mesh technique. The effects of LOS, rotor spacing and RPM are analyzed. Following conclusions can be drawn from this paper:

- (1) In forward flight, the lift–drag ratio of the rigid coaxial rotor increases first and then decreases with the increase of LOS. This is the combined result of two aspects. One is that the high dynamic pressure at the advancing side can be fully utilized via LOS, improving the aerodynamic efficiency. The other is that when the lift–offset is achieved, the offset of drag is also brought correspondingly. And this leads to larger rotor drag. The optimum LOS for lift–drag ratio varies with the advance ratio.
- (2) At large advance ratio, interactions of the rigid coaxial rotor are much weak, except the blade–meeting interaction, which leads to impulsive blade loads. It is typically shown on the thrust of the upper blade at the retreating side (270°), as the flow field is dominated by the lower blade with larger dynamic pressure and stronger load at the advancing side (90°). The interaction is mainly formatted by the strong-gradient flow field induced by the lower blade, and turns stronger with the increase of advance ratio and LOS.
- (3) The blade–meeting interaction is much sensitive to rotor spacing and RPM. With a larger spacing, the upper blade is further away from the strong-gradient region of

the lower blade. Thus, the interaction is sharply weakened. At a higher RPM, the gradient of the flow field above the advancing lower blade is enhanced, leading to stronger interaction. Based on the parametric analysis of this paper, our future work will be focused on the parameter design of rigid coaxial rotor and blade shape optimization to reduce the aerodynamic unsteady loads and aerodynamic noise.

Acknowledgements This work was supported by the National Natural Science Foundation of China (No. 12102154), and the Foundation of Key Laboratory of Aerodynamic Noise Control (No. ANCL20200203).

Declarations

Conflict of Interest The authors declare that they have no known competing financial interests or personal relationships that could have appeared to influence the work reported in this paper.

References

1. Ho JC, Yeo H (2020) Analytical study of an isolated coaxial rotor system with lift offset. *Aerosp Sci Technol* 100:105818
2. Bagai A (2008) Aerodynamic design of the X2 technology demonstrator main rotor blade. Paper presented at the 64th American Helicopter Society Annual Forum, Montréal, Canada, Apr 29–May 1
3. Burgess RK (2004) The ABC™ Rotor – A historical perspective. Paper presented at the 60th American Helicopter Society Annual Forum, Baltimore, MD, USA, 7–10 June
4. Ho JC, Yeo H (2020) Rotorcraft comprehensive analysis calculations of a coaxial rotor with lift offset. *Int J Aeronaut Space* 21(2):418–438
5. Schmaus JH, Chopra I (2015) Aeromechanics for a high advance ratio coaxial helicopter. Paper presented at the 71st American Helicopter Society Annual Forum, Virginia Beach, VA, USA, 5–7 May
6. Schmaus JH, Chopra I (2017) Aeromechanics of rigid coaxial rotor models for wind-tunnel testing. *J Aircr* 54(4):1486–1497
7. Go J-I, Kim D-H, Park J-S (2017) Performance and vibration analyses of lift-offset helicopters. *Int J Aerosp Eng* 2017:1–13
8. Feil R, Rauleder J, Cameron CG, Sirohi J (2019) Aeromechanics analysis of a high-advance-ratio lift-offset coaxial rotor system. *J Aircr* 56(1):166–178
9. Kwon Y-M, Park J-S, Wie S-Y, Kang HJ, Kim D-H (2021) Aeromechanics analyses of a modern lift-offset coaxial rotor in high-speed forward flight. *Int J Aeronaut Space* 22(2):338–351
10. Hayami K, Sugawara H, Tanabe Y, Kameda M (2020) Numerical investigation of aerodynamic interference on coaxial rotor. Paper presented at the AIAA Scitech 2020 Forum, Orlando, FL, 6–10 Jan
11. Lakshminarayan VK, Baeder JD (2010) Computational investigation of microscale coaxial-rotor aerodynamics in hover. *J Aircr* 47(3):940–955
12. Qi H, Xu G, Lu C, Shi Y (2019) A study of coaxial rotor aerodynamic interaction mechanism in hover with high-efficient trim model. *Aerosp Sci Technol* 84:1116–1130
13. Qi H, Xu G, Lu C, Shi Y (2019) Computational investigation on unsteady loads of high-speed rigid coaxial rotor with high-efficient trim model. *Int J Aeronaut Space* 20(1):16–30
14. Wang B, Cao C, Zhao Q, Yuan X, Zhu Z (2021) Aeroacoustic characteristic analyses of coaxial rotors in hover and forward flight. *Int J Aeronaut Space* 22(6):1278–1292
15. Park SH, Kwon OJ (2021) Numerical study about aerodynamic interaction for coaxial rotor blades. *Int J Aeronaut Space* 22(2):277–286
16. Singh R, Kang H, Cameron C, Sirohi J (2016) Computational and Experimental Investigations of Coaxial Rotor Unsteady Loads. Paper presented at the 54th AIAA Aerospace Sciences Meeting, San Diego, California, USA, 4–8 Jan
17. Klimchenko V, Sridharan A, Baeder JD (2017) CFD/CSD study of the aerodynamic interactions of a coaxial rotor in high-speed forward flight. Paper presented at the 35th AIAA Applied Aerodynamics Conference, Denver, Colorado, USA, 5–9 June
18. Jia Z, Lee S (2020) Impulsive loading noise of a lift-offset coaxial rotor in high-speed forward flight. *AIAA J* 58(2):687–701
19. Jia Z, Lee S (2021) Aerodynamically induced noise of a lift-offset coaxial rotor with pitch attitude in high-speed forward flight. *J Sound Vib* 491:115737
20. Silwal L, Raghav V (2020) Preliminary study of the near wake vortex interactions of a coaxial rotor in hover. Paper presented at the AIAA Scitech 2020 Forum, Orlando, FL, USA, 6–10 Jan
21. Ye Z, Xu G, Shi Y, Xia R (2017) A high-efficiency trim method for CFD numerical calculation of helicopter rotors. *Int J Aeronaut Space* 18(2):186–196
22. Zhao QJ, Zhao GQ, Wang B, Wang Q, Shi YJ, Xu GH (2018) Robust Navier-Stokes method for predicting unsteady flowfield and aerodynamic characteristics of helicopter rotor. *Chin J Aeronaut* 31(2):214–224
23. Pomin H, Wagner S (2002) Navier-Stokes analysis of helicopter rotor aerodynamics in hover and forward flight. *J Aircr* 39(5):813–821
24. Roe PL (1981) Approximate Riemann solvers, parameter vectors, and difference schemes. *J Comput Phys* 43:357–372
25. Van Leer B (1979) Towards the ultimate conservative difference scheme. V. A second-order sequel to Godunov's method. *J Comput Phys* 32(1):101–136
26. Spalart P, Allmaras S (1992) A one-equation turbulence model for aerodynamic flows. Paper presented at the 30th Aerospace Sciences Meeting and Exhibit, Reno, NV, USA, 6–9 Jan
27. Yoon S, Jameson A (1988) Lower-upper Symmetric-Gauss-Seidel method for the Euler and Navier-Stokes equations. *AIAA J* 26(9):1025–1026
28. Passe BJ, Sridharan A, Baeder JD (2015) Computational investigation of coaxial rotor interactional aerodynamics in steady forward flight. Paper presented at the 33rd AIAA Applied Aerodynamics Conference, Dallas, TX, USA, 22–26 Jun
29. Zhao JG, He CJ (2010) A viscous vortex particle model for rotor wake and interference analysis. *J Am Helicopter Soc* 55(1):12007–1200714
30. Dinkeldein RC (1954) Wind-tunnel studies of the performance of multirotor configurations. NACA Technical Note, NACA-TN-3236
31. Barbely N, Novak L, Komerath N (2016) A study of coaxial rotor performance and flow field characteristics. Paper presented at the American Helicopter Society Technical Meeting, Fisherman's Wharf, San Francisco, USA, 20–22 Jan

Publisher's Note Springer Nature remains neutral with regard to jurisdictional claims in published maps and institutional affiliations.